Published in final edited form as:
Cancer Res. 2012 August 1; 72(15): 3725–3734. doi:10.1158/0008-5472.CAN-11-3943.

Prognostic PET ^{18}F-FDG uptake imaging features are associated with major oncogenomic alterations in patients with resected non-small cell lung cancer

Viswam S. Nair[1,†], **Olivier Gevaert**[4,†], **Guido Davidzon**[3], **Sandy Napel**[4], **Edward E. Graves**[5], **Chuong D. Hoang**[2,6], **Joseph B. Shrager**[2,6], **Andrew Quon**[3], **Daniel L. Rubin**[4], and **Sylvia K. Plevritis**[4]

[1]Division of Pulmonary & Critical Care Medicine, Stanford University School of Medicine

[2]Division of Thoracic Surgery, Stanford University School of Medicine

[3]Division of Nuclear Medicine, Stanford University School of Medicine

[4]Department of Radiology, Stanford University School of Medicine

[5]Department of Radiation Oncology, Stanford University School of Medicine

[6]Veterans Administration Palo Alto Health Care System

Abstract

Although ^{18}F-2-fluoro-2-deoxyglucose (FDG) uptake during positron emission tomography (PET) predicts post-surgical outcome in patients with non-small-cell lung cancer (NSCLC), the biologic basis for this observation is not fully understood. Here we analyzed 25 tumors from NSCLC patients to identify tumor ^{18}F-FDG PET uptake features associated with gene expression signatures and survival. Fourteen quantitative PET imaging features describing FDG uptake were correlated with gene expression for single genes and co-expressed gene clusters (metagenes). For each FDG uptake feature, an associated metagene signature was derived and a prognostic model was identified in an external and tested in a validation cohort of NSCLC patients. Four of 8 single genes associated with FDG uptake (LY6E, RNF149, MCM6, FAP) were also associated with survival. The most prognostic metagene signature was associated with a multivariate FDG uptake feature (SUV_{max}, $SUV_{variance}$ and SUV_{PCA2}), each highly associated with survival in the external (HR 5.87, confidence interval [CI] 2.49-13.8) and validation (HR 6.12, CI 1.08-34.8) cohorts, respectively. Cell cycle, proliferation, death, and self-recognition pathways were altered in this radiogenomic profile. Together, our findings suggest that leveraging tumor genomics with an expanded collection of PET-FDG imaging features may enhance our understanding of FDG uptake as an imaging biomarker beyond its association with glycolysis.

Keywords

Lung cancer; FDG; PET; genomics; prognosis

Correspondence: Sylvia K. Plevritis PhD Department of Radiology Stanford University School of Medicine Stanford, CA, 94305 Phone: (650) 725-4936 Fax: (650) 723-5795 sylvia.plevritis@stanford.edu.
[†]VSN and OG contributed equally to this work

Conflicts: None to declare for all authors

Introduction

Non-small cell lung cancer (NSCLC) remains the number one cause of cancer related mortality for men and women in the U.S, and its prevalence continues to increase worldwide.(1) Despite potentially curative resection in early-stage NSCLC, survival remains sub-optimal and recurrence rates are high.(2)

^{18}F-2-fluoro-2-deoxyglucose (FDG) positron emission tomography (PET) imaging is currently the standard of care for pre-operative staging of disease in NSCLC, and multiple investigations suggest that the intensity of FDG uptake in the tumor prior to surgery is a useful biomarker for tumor aggressiveness and patient outcome post-operatively.(3-5) This is an important finding since PET imaging is non-invasive, cost-effective, and routinely performed for patients pre-operatively.(6-9)

FDG-PET uptake is governed by GLUT transporter uptake and metabolized to an inert intracellular product by a key regulatory enzyme in glycolysis, Hexokinase-2 (HK2).(10) The biologic basis for the utility of FDG as a biomarker is not fully understood, but up-regulated glycolysis that results in increased FDG uptake has been associated with tumor growth, metastasis and immune evasion.(11-14) Recently, a key driver that seemingly promotes a less favorable cellular energy profile was discovered (Pyruvate kinase isoenzyme M2 [PKM2]),(15-17) and has been implicated with other major genes involved in oncogenesis that may help to explain a mechanistic switch to a glycolytic phenotype.(18)

To date, no studies have examined differential genome wide expression across varying FDG uptake levels in NSCLC. We explored this relationship in a cohort of patients with NSCLC to identify individual genes and gene expression signatures associated with prognostically relevant FDG uptake features.

Methods

Study design

We employed a novel biocomputational approach to associate gene expression with prognostic FDG uptake features (Figure 1) using 3 cohorts (study, external and validation cohorts). Use of all three cohorts allowed us to: (i) associate FDG uptake features to gene expression, (ii) generate a model of image features in terms of their gene expression (study cohort), (iii) identify prognostic gene signatures from this model (external cohort), and finally (iv) examine whether image features associated with prognostic gene sets were predictive of clinical outcome (validation cohort). To build prognostic gene expression signatures associated with FDG uptake image features, we applied our previously described radiogenomics strategy.(19)

Study, external and validation cohorts

For the study cohort, a group of patients with surgically resected NSCLC between 2008 and 2010 from two medical centers were retrospectively identified. All patients had pre-operative PET-CT scans analyzed for tumor FDG uptake features matched with excised tumor specimens subjected to global gene expression analysis. Patients receiving neo-adjuvant therapy were excluded and follow-up data was not available for the study cohort since these cases were taken from recent operative specimens. For the external cohort we used data from a previous study that modeled gene expression and outcome in patients with NSCLC (GSE8894).(20) For the validation cohort we examined patients with resected, limited stage NSCLC from 2003 to 2010 who underwent treatment naïve, pre-operative PET imaging. Death was assessed using the National Death Index (www.cdc.gov/nchs/ndi) and

patients not dead were assumed to be alive at the time of data extraction (June, 2011). All work was performed with the IRB authorization of both participating centers.

PET acquisition and FDG uptake feature extraction in study and validation cohorts

PET/CT images were acquired using either a LS PET/CT (slice thickness 3 to 5 mm) at Stanford or GE Discovery VCT (slice thickness 3.75 mm) at the Veterans Administration Palo Alto Health Care System (VAPAHCS). At Stanford, patients fasted for a minimum of eight hours, a dose of 12-17 millicuries (mci) of FDG was administered, and patients were scanned from the skull base to mid-thigh using multiple bed positions every 5 minutes approximately 45 to 60 minutes after injection. Prior to injection of FDG, patients who had a blood glucose level of >180 mg/dL were excluded. At the VAPAHCS, patients fasting for 6 hours had FDG injected to a target of 15 mci at time of scan, which ranged from 60 to 120 minutes after injection, and those patients who had a blood glucose of level of >200 mg/dL were rescheduled. Patients were scanned from skull to mid-thigh using multiple bed positions every 2 to 3 minutes. CT attenuated data was reconstructed using ordered subset expectation maximization (OSEM) for both scanner sites.

FDG uptake was quantified using the maximum standard uptake value (SUV_{max}) by a certified nuclear medicine physician (AQ). The region-of-interest (ROI) for each nodule was drawn using the trans-axial image that was thought to represent the most FDG avid portion around the entire lesion and the maximum SUV pixel within the ROI (SUV_{max}) was recorded. Partial volume correction was not used for this interpretation. All DICOM images for both study and validation cohorts were then imported into an imaging feature extraction program, RT_Image (http://rtimage.sourceforge.net). FDG uptake metrics were calculated after co-registration with CT images of the tumor and then by defining an automated ROI on the PET image using a region-growing algorithm bounded by a standard threshold uptake above background with a lower bound set at 50% of the maximum value within the ROI. (21)

Fourteen metrics of interest related to SUV were recorded: SUV minimum, maximum, mean, median and percentile (75 and 90) features were extracted to define the intensity of FDG uptake in tumor; SUV standard deviation, variance, skew and kurtosis features were extracted to measure the variation in FDG uptake across the tumor; and metabolic tumor volume (MTV), registration points (number of voxels used to define the MTV), area and total glycolytic volume (TGV) quantified the spatial extent of FDG uptake. TGV is represented in this study as the product of SUV_{mean} and metabolic volume and represents the “integrated” metabolic uptake across the tumor.(22)

Comparison of study and validation cohorts

Basic descriptive clinical, pathologic and imaging characteristics were tabulated for study and validation cohorts. Continuous variables with median and interquartile range or categorical variables with percent were calculated. Differences between the study and validation cohorts were assessed using a student's t-test for continuous variables or a Chi-squared or Fisher's exact test (for less than five data points in a level) for categorical variables.

Gene expression microarray data

Tumors from the study cohort were processed from a 3–5 mm cross-section after removal of fibrotic or necrotic areas during surgical excision (CDH/JS). Tumor tissue was snap frozen within 30 minutes and extracted to RNA using standard commercial kits. Genome wide arrays were processed by the Stanford Functional Genomics Facility using Illumina™ Whole Genome Bead Chips (Human HT-12). Microarray data was filtered based on a

significant detection call in at least 60% of the samples and log transformed using quantile normalization to account for array variation. Microarray data was submitted to GEO under accession number GSE28827.

Association of FDG uptake features and gene expression

Basic correlations amongst FDG uptake features and for FDG uptake features with gene expression were performed using a Spearman-rank correlation test. Significance of microarrays (SAM) analysis was performed to define genes significantly associated with FDG uptake metrics. Because of the potential for false positive associations due to multiple comparisons we used the False Discovery Rate (q-value <0.05) to assess statistical significance.(23) In addition, because single gene associations with image features are more prone to noise, a clustering method to reduce the dimensionality of the microarray data was employed in addition to univariate SAM analysis.(19) We clustered the microarray data using an iterative k-means clustering algorithm with 200 iterations and a coherence of 0.75; these settings were determined such that the average cluster homogeneity in external data sets was maximal,(20, 24) where cluster homogeneity was defined as the average correlation between each member of the cluster within the cluster centroid. This clustering algorithm resulted in 102 clusters that were then filtered based on a homogeneity of at least 0.30 in one of two external data sets,(19, 24) to yield 56 high quality clusters, defined in this study as metagenes, for further analysis.[12]

PCA analysis of FDG uptake features

We examined the principal components defining FDG uptake for the 14 features extracted to determine which features accounted for most of the variability of FDG uptake. Each principal component was defined as a linear combination of the 14 original features and could be interpreted based on the weights associated with each of these features. We restricted our analysis to the first three principal components and incorporated these new features to the study cohort data set for further analyses.

Predicted FDG uptake features and their association with overall survival

Individual genes associated with FDG uptake in the study cohort were directly analyzed in the external cohort for their association to clinical outcomes. In addition, a multivariate model of FDG uptake features in the study cohort for each of the 14 features studied was built by a linear combination of metagenes to further examine the likely underlying biology of the features and their association with outcome in the external cohort. The accuracy of gene signatures to predict FDG uptake features was determined by examining the absolute difference in the predicted FDG uptake feature with the actual imaging feature value.[12] Only signatures with an accuracy of greater than 0.70 were carried forward for further analysis and analyzed with outcome in the external dataset. We refer to these features, now defined in terms of a gene signature, as “predicted FDG uptake features” and denote them with a prefix “p” (i.e. *p*SUV_{max} represents the prognostic gene signature associated with SUV_{max}). Kaplan-Meier (KM) curves were dichotomized at the median gene expression value and unadjusted Cox-proportional hazards (CPH) testing was performed to assess the prognostic significance for predicted FDG uptake features and individual genes that were highly correlated to FDG features. We also performed Lasso CPH modeling(25) with 10 fold cross-validation to identify a multivariate signature of multiple predicted FDG uptake features whose gene expression signature was associated with outcome, creating the “multivariate-SUV” model.

Validation of prognostic FDG uptake features

We studied FDG uptake features associated with prognostic gene signatures (i.e. *p*FDG features) from the external cohort in a validation cohort which consisted of 84 patients with PET imaging and survival data. We analyzed extracted FDG uptake features, computed their principal components, and derived the multivariate-SUV model by Lasso Cox-proportional hazards (CPH) analysis. To describe outcomes for these features, Kaplan-Meier (KM) curves were dichotomized at the median FDG uptake feature value and unadjusted CPH testing was performed. Lastly, we analyzed the prognostic significance of age, tumor size and stage for the external and validation cohorts separately, followed by multivariate analyses with univariately-derived prognostic imaging features, to determine whether these imaging features added statistically significant independent information to prognosis in both cohorts.

Gene enrichment analysis of predicted FDG uptake features

We used a hyper-geometric test with multiple testing correction and FDR(26) for metagene enrichment analysis using gene set collections from GeneSigDb (compbio.dfci.harvard.edu/genesigdb), the NIH Database for Annotation, Visualization and Integrated Discovery (DAVID http://david.abcc.ncifcrf.gov),(27) MSigDb (www.broadinstitute.org/gsea/Msigdb), (28, 29) and Reactome (www.reactome.org).(30) We then framed the biologic context of these genes signatures by mapping them to known molecular pathways (IPA™). For this study, gene expression magnitude and direction for network visualization was derived using the z-score from univariate SAM analysis in the external cohort with survival as the dependent variable.

All analyses were performed using MATLAB™ (Mathworks Inc., Natick, MA), R (v. 2.11.1), SAS™ (v9.2, SAS, Cary, NC) and IPA™ (v9.0, Ingenuity, Redwood City, CA).

Results

Study, external and validation cohorts

Twenty-five tumors from 25 patients with a median age of 71 years (range 50–86), who had predominantly early-stage adenocarcinoma with lobectomy performed were identified for the study cohort (Table 1). The median time to operation from PET acquisition was 27 days and median tumor diameter (in the largest measured dimension) was 2.3 cm. The external cohort consisted of 63 patients with adenocarcinoma and a median age of 60 years. For the external cohort, eighty-one percent of patients were stage I-II with a median tumor diameter of 3.5 cm, follow-up of 42 months and 24 (38%) deaths in follow-up (Supplement 1). The validation cohort consisted of 84 patients that had similar patient characteristics to the study cohort discounting gender (Table 1), SUV_{median} and SUV_{min}, for which significant differences existed among variables (Table 1). Median follow-up time in the validation cohort was 38 months, during which time 21 (25%) patients died.

FDG uptake measurements

Blood glucose (mg/dL), injected dose (millicuries) and time to scan (minutes) were similar between the study and validation cohorts except for time to scan, which was longer in the study cohort (Table 1). ROI segmentation and feature extraction was fully automated for all patients in the discovery cohort using RT_Image, but nine of 84 patients (11%) in the validation group required manual override due to improper segmentation from the RT_Image algorithm.

In the study cohort, median calculated SUV_{max} from RT_Image was 3.2 (range 0.98–30), which agreed well with human observation by a certified nuclear medicine physician (AQ,

r=0.91). FDG uptake features between study and validation cohorts were reasonably similar in distribution but differed significantly for SUV_{median} and SUV_{min} (Table 1). SUV_{max} was highly correlated (r>0.8) with mean, median, standard deviation, variance, total glycolytic volume and percentile metrics, moderately correlated (r>0.6) with minimum, area, volume and points metrics, and modestly correlated with skew and kurtosis features (r=0.48 and 0.32 respectively).

PCA Analysis of FDG uptake features

The first three principal components explained 96% of the image feature variance for the study cohort and defined new FDG uptake features. The first principal component was dominated by traditional point estimates of FDG uptake features (SUV_{max}, SUV_{mean}, SUV_{median}) and spatial metrics (SUV_{points}, SUV_{MTV}, SUV_{area}). The second and third components were associated with $SUV_{kurtosis}$ and SUV_{skew}, measures of the shape of FDG uptake distribution, as well as SUV_{min}. These three principal components were added into a subsequent analysis with the initial fourteen imaging features to examine their association with survival in the external cohort.

Gene expression and FDG uptake feature associations in the study cohort

In the study cohort, 37,798 assayed genes were filtered according to a 60% call rate (i.e. only those genes appearing in more than 60% of samples were carried forward) to yield 8,238 present genes. After applying a variance filter described in the methods section, approximately half of these genes were included for further analysis. Eight of these 4,261 single genes were strongly associated with seven different FDG uptake features by SAM analysis (Table 2). SUV_{mean} was significantly associated with five genes and SUV_{mean} and SUV_{skew} were the only FDG uptake features uniquely associated with single genes.

Fifty-six high-quality gene clusters (representing 2300 individual genes, per Methods) were correlated to the FDG uptake features using SAM analysis. Eight of these meta-genes consisting of 240 individual genes were significantly associated with seven different FDG uptake features (FDR = 0), and SUV_{max} and SUV_{mean} features were enriched in extracellular matrix components in the study cohort (Table 2). Imaging features SUV_{skew}, SUV_{min} and SUV_{TGV} were uniquely associated with meta-genes enriched in protein and nucleic acid catabolism, as well as tumor suppressor pathways.

Predicted FDG uptake features and their association with survival

Predicted FDG uptake imaging features with an acceptable accuracy were carried forward to subsequent survival analysis (Table 3). All features passed this quality control except the 3rd PCA (SUV_{PCA3}). Predicted $p$$SUV_{max}$, $p$$SUV_{mean}$, $p$$SUV_{min}$, $p$$SUV_{variance}$ and $p$$SUV_{PCA2}$ were significantly associated with survival in the external cohort (Table 4). A multivariate model of predicted FDG uptake features associated with survival identified $p$$SUV_{max}$,, $p$$SUV_{variance}$, and $p$$SUV_{PCA2}$ as the top three prognostic FDG uptake features for predicting poor outcomes, with associated weights of 0.260, -0.281 and 0.148 respectively; we refer to this model as the multivariate-SUV model. Compared to the univariate FDG uptake features, the multivariate-SUV model yielded greatest prognostic value in the external cohort (HR 5.87, CI 2.59–13.8). For single genes, four of eight genes associated with FDG uptake from the study cohort were significantly associated with survival in the external dataset (Table 4).

Validation of the prognostic FDG uptake features

We validated the significance of the predicted FDG uptake features that were associated with prognostic gene signatures on outcome in an additional 84 patient cohort with image data and survival data (Table 4). Both SUV_{max} (HR 1.05, CI 1.00–1.10) and the

multivariate-SUV model (HR 6.12, CI 1.08–34.8) were significantly associated with survival by univariate CPH analysis and Kaplan-Meier plot (Figure 2). The prognostic significance of SUV_{mean} (p-value 0.08), SUV_{PCA2} (p-value 0.08), $SUV_{variance}$ (p-value 0.16) and SUV_{min} (p-value 0.62) were not confirmed in the validation cohort, although the first two features maintained a strong trend with outcome ($p<0.10$).

Incorporating clinical variables with prognostic FDG uptake features

In a univariate analysis, tumor size (cm) and stage (I-IV) were prognostically significant in both the external and validation cohorts (Supplement 6). After adjusting for the clinical variables tumor size, stage and age, *p*SUV_{max} was found to be independently significant for predicting worse outcome in the external cohort (Supplement 6). Adjusted point estimates for the hazard ratios associated with SUV_{max} in the validation cohort, as well as the multivariate-SUV feature in the external and validation cohorts, were all greater than 1.0 but not statistically significant (Supplement 6).

Gene network analysis

We further utilized network analysis and gene enrichment databases to inform us of important functional relationships between imaging features and gene expression for SUV_{max} and the multivariate-SUV model. SUV_{max}, comprising 15 metagenes and 508 individual genes, was enriched in cell cycle (CDK2NA–p16) and acetylation (histone) pathways with network analysis showing a prominent NFKB node (Supplement 7). Of the 1,367 genes comprising the multivariate-SUV model, 484 were duplicated between features, leaving 883 unique genes to map for network analysis. Multiple important oncogenic pathways including cell proliferation (STAT1, PKA, FGF), cell cycle (CCNB, CCND, CEPBA), apoptosis (BAX, Caspase, BIRC5), endocytosis (COP–Clathrin pathways), cell recognition (HLA-MHC) and oxidative phosphorylation (SLC25, Cytochrome C, COX) were distinct nodes in this network (Supplement 7).

Discussion

Aberrant cell signaling, proliferation and immortality are well known hallmarks of cancer. (31) We show here that gene expression related to prognostic FDG uptake features was enriched in these canonical pathways. Emerging hallmarks of cancer–including cell bioenergetics, inflammation and immune evasion may also play an important role in defining FDG uptake as a global marker of poor prognosis in patients with resected NSCLC according to our analysis. Finally, increasing SUV_{max} is well established to be associated with poor patient outcome(3-5) and our analysis suggests that NFKB signaling is a key molecular correlate for this imaging biomarker. This is a provocative finding since NFKB signaling is activated downstream by lactate production from glycolysis and–like FDG uptake–is increased in inflammatory and malignant diseases.(32)

By employing a computational design for this study, we examined multiple prognostic FDG uptake imaging features with genome wide expression from NSCLC tumors. After accounting for multiple comparisons with FDR analysis ($q<0.05$) we show that novel FDG uptake features were associated with distinct genes and gene signatures, less related (ie, correlated) features were associated with different genes and gene signatures, and in combination features provided a more prognostic model than any one feature alone.

One previous study has investigated gene expression across varying degrees of FDG uptake in breast cancer, as defined by SUV_{max}, and glycolytic genes were remarkably absent from the most highly significant associations–as was the case in our study (Supplement 8).(33) A follow-up to that study focusing on cell bio-energetics found that glycolytic pathways are

up-regulated in the context of other major tumor pathways but are not the most highly enriched pathways.(34) Interestingly, this follow-up study focused on another important driver of oncogenesis, c-MYC, and related it to FDG uptake. In contrast, our study's prognostic multivariate-SUV feature was associated with other major drivers of oncogenesis, although we also found MYC related pathways were enriched during ontology analysis (Supplements 3 and 4).

Models like these may deepen the utility, and our understanding, of FDG uptake as a biomarker and may provide additional insight at the genomic level for a tumor phenotype defined by heterogeneous FDG uptake at the imaging level. The Warburg Effect was initially described over 80 years ago and postulates that tumors undergo glycolysis preferentially despite adequate intracellular oxygen tension.(35, 36) Although Warburg believed this was a result of mitochondrial dysfunction, we now know that tumor glycolysis can proceed with functional cellular mitochondria and in fact may be an adaptive response for tumor survival.(10, 11, 37) Furthermore, studies have recently linked glycolysis in cancer to more widespread dysregulation of cell bioenergetics,(38-40) suggesting that FDG uptake may be a surrogate for more than glycolysis alone and perhaps a lens through which one can view global tumor bioenergetics.

This study has limitations. To identify the prognostic significance of FDG features and their associated gene signatures, the ideal cohort would typically consist of hundreds of patients with: (i) genomic profiling of their resected tumor, (ii) PET imaging of the tumor prior to resection and (iii) long term follow-up. Because such large cohorts are not yet commonly available, we present and implemented a novel technique that integrates the 3 data types (namely, gene expression, imaging and survival data) from 3 different cohorts.

We did not apply a correction of FDG-PET signal that may sometimes be required for tumors that approach the resolution of the PET scanner (~1.5–2.0 cm)–known as partial volume effect correction–to our data.(41, 42) While some studies have shown this can have a significant effect on traditionally employed metrics of uptake, such as SUV_{max} and SUV_{mean},(43) the effect of correcting for more novel features, such as SUV_{MTV} and SUV_{skew}, is unresolved to date.(44) In addition to the above intra-scan variation, inter-scan variation between PET scanners exists, can add to imprecision for feature quantification, and should be accounted for in future multi-center studies.(45)

Although our sample was predominantly adenocarcinoma, there was some heterogeneity in histology, which is well known to effect both FDG uptake and gene expression.(46, 47) We may not have exploited the full gamut of prognostic imaging features we derived using RT_Image since we were interested in examining only those FDG uptake features that were associated with prognostic gene signatures. Lastly, the added significance of prognostic imaging features and their associated gene profiles compared to traditional clinical variables of prognosis was marginal, possibly due to the sample size and heterogeneity of the cohorts examined. Yet, our results indicate that larger studies are warranted to evaluate the prognostic significance of a broader characterization of FDG uptake features and to assess the relationship of FDG uptake to molecular processes beyond glycolysis.

Conclusion

Utilizing gene leveraging techniques can harness the power of the public domain for expediting studies of radiogenomic biomarkers. A computational approach to understanding gene expression correlates of aggressive NSCLC as defined by prognostic ^{18}F-FDG uptake features may offer new insights into tumor biology. Our methods require further study in

other human cancers and larger, homogeneous cohorts of NSCLC patients with standardized gene expression, imaging and clinical data.

Supplementary Material

Refer to Web version on PubMed Central for supplementary material.

Acknowledgments

The authors would like to thank Yue Xu for processing tissues for genomic analysis, Sanjiv S. Gambhir for his insights and comments relating to this work, as well as Frezghi Habte and Khun Visith Keu for providing data relating to inter-calibration of PET scanners. We also thank Dr. S.H. Kim for sharing additional clinical data related to his gene expression data set.

Grant Support: This research was supported by the Information Sciences in Imaging at Stanford and the Center for Cancer Systems Biology (U54 CA149145, OG & SKP; R01 CA16025, SKP) and the Division of Pulmonary & Critical Care Medicine at Stanford University School of Medicine (T32 HL007948, VSN). Additional support for VSN was provided by the Lung Cancer Research Foundation and the CHEST Foundation California Chapter Clinical Research Award. OG is a fellow of the Fund for Scientific Research Flanders (FWO-Vlaanderen), an Honorary Fulbright Scholar of the Commission for Educational Exchange between the United States of America, Belgium and Luxembourg, and a Henri Benedictus Fellow of the King Baudouin Foundation and the Belgian American Educational Foundation (BAEF). Database support for this project was provided by the Stanford NIH/NCRR CTSA UL1 RR025744 and NCI 5P30CA124435 awards.

References

1. Jemal A, Siegel R, Xu J, Ward E. Cancer Statistics, 2010. CA Cancer J Clin. 2010
2. Pignon JP, Tribodet H, Scagliotti GV, Douillard JY, Shepherd FA, Stephens RJ, et al. Lung adjuvant cisplatin evaluation: a pooled analysis by the LACE Collaborative Group. J Clin Oncol. 2008; 26(21):3552–9. [PubMed: 18506026]
3. Berghmans T, Dusart M, Paesmans M, Hossein-Foucher C, Buvat I, Castaigne C, et al. Primary tumor standardized uptake value (SUVmax) measured on fluorodeoxyglucose positron emission tomography (FDG-PET) is of prognostic value for survival in non-small cell lung cancer (NSCLC): a systematic review and meta-analysis (MA) by the European Lung Cancer Working Party for the IASLC Lung Cancer Staging Project. J Thorac Oncol. 2008; 3(1):6–12. 01243894-200801000-00003 [pii]. PubMed PMID: 18166834. [PubMed: 18166834]
4. Nair VS, Barnett PG, Ananth L, Gould MK. PET scan 18F-fluorodeoxyglucose uptake and prognosis in patients with resected clinical stage IA non-small cell lung cancer. Chest. 2010; 137(5): 1150–6. [PubMed: 20038738]
5. Paesmans M, Berghmans T, Dusart M, Garcia C, Hossein-Foucher C, Lafitte JJ, et al. Primary tumor standardized uptake value measured on fluorodeoxyglucose positron emission tomography is of prognostic value for survival in non-small cell lung cancer: update of a systematic review and meta-analysis by the European Lung Cancer Working Party for the International Association for the Study of Lung Cancer Staging Project. J Thorac Oncol. 2010; 5(5):612–9. [PubMed: 20234323]
6. Gould MK, Kuschner WG, Rydzak CE, Maclean CC, Demas AN, Shigemitsu H, et al. Test performance of positron emission tomography and computed tomography for mediastinal staging in patients with non-small-cell lung cancer: a meta-analysis. Ann Intern Med. 2003; 139(11):879–92. [PubMed: 14644890]
7. Gould MK, Sanders GD, Barnett PG, Rydzak CE, Maclean CC, McClellan MB, et al. Cost-effectiveness of alternative management strategies for patients with solitary pulmonary nodules. Ann Intern Med. 2003; 138(9):724–35. [PubMed: 12729427]
8. Gambhir SS, Shepherd JE, Shah BD, Hart E, Hoh CK, Valk PE, et al. Analytical decision model for the cost-effective management of solitary pulmonary nodules. J Clin Oncol. 1998; 16(6):2113–25. [PubMed: 9626211]
9. van Tinteren H, Hoekstra OS, Smit EF, van den Bergh JH, Schreurs AJ, Stallaert RA, et al. Effectiveness of positron emission tomography in the preoperative assessment of patients with

suspected non-small-cell lung cancer: the PLUS multicentre randomised trial. Lancet. 2002; 359(9315):1388–93. [PubMed: 11978336]

10. Mathupala SP, Ko YH, Pedersen PL. Hexokinase-2 bound to mitochondria: cancer's stygian link to the “Warburg Effect” and a pivotal target for effective therapy. Semin Cancer Biol. 2009; 19(1): 17–24. [PubMed: 19101634]
11. Frezza C, Gottlieb E. Mitochondria in cancer: not just innocent bystanders. Semin Cancer Biol. 2009; 19(1):4–11. [PubMed: 19101633]
12. Shanmugam M, McBrayer SK, Rosen ST. Targeting the Warburg effect in hematological malignancies: from PET to therapy. Curr Opin Oncol. 2009; 21(6):531–6. [PubMed: 19587591]
13. Semenza GL. Hypoxia and cancer. Cancer Metastasis Rev. 2007; 26(2):223–4. [PubMed: 17404692]
14. Koppenol WH, Bounds PL, Dang CV. Otto Warburg's contributions to current concepts of cancer metabolism. Nature reviews Cancer. 2011; 11(5):325–37.
15. Christofk HR, Vander Heiden MG, Harris MH, Ramanathan A, Gerszten RE, Wei R, et al. The M2 splice isoform of pyruvate kinase is important for cancer metabolism and tumour growth. Nature. 2008; 452(7184):230–3. [PubMed: 18337823]
16. Christofk HR, Vander Heiden MG, Wu N, Asara JM, Cantley LC. Pyruvate kinase M2 is a phosphotyrosine-binding protein. Nature. 2008; 452(7184):181–6. [PubMed: 18337815]
17. Vander Heiden MG, Locasale JW, Swanson KD, Sharfi H, Heffron GJ, Amador-Noguez D, et al. Evidence for an alternative glycolytic pathway in rapidly proliferating cells. Science. 2010; 329(5998):1492–9. [PubMed: 20847263]
18. Yang W, Xia Y, Ji H, Zheng Y, Liang J, Huang W, et al. Nuclear PKM2 regulates beta-catenin transactivation upon EGFR activation. Nature. 2011; 480(7375):118–22. [PubMed: 22056988]
19. Gevaert O XJ, Hoang C, Leung A, Xu Y, Quon A, et al. Identification of prognostic imaging biomarkers for non-small cell lung cancer by leveraging public gene expression microarray data. Radiology. 2012
20. Lee ES, Son DS, Kim SH, Lee J, Jo J, Han J, et al. Prediction of recurrence-free survival in postoperative non-small cell lung cancer patients by using an integrated model of clinical information and gene expression. Clin Cancer Res. 2008; 14(22):7397–404. [PubMed: 19010856]
21. Graves EE, Quon A, Loo BW Jr. RT_Image: an open-source tool for investigating PET in radiation oncology. Technol Cancer Res Treat. 2007; 6(2):111–21. [PubMed: 17375973]
22. La TH, Filion EJ, Turnbull BB, Chu JN, Lee P, Nguyen K, et al. Metabolic tumor volume predicts for recurrence and death in head-and-neck cancer. Int J Radiat Oncol Biol Phys. 2009; 74(5): 1335–41. [PubMed: 19289263]
23. Tibshirani R, Hastie T, Narasimhan B, Chu G. Diagnosis of multiple cancer types by shrunken centroids of gene expression. Proc Natl Acad Sci U S A. 2002; 99(10):6567–72. [PubMed: 12011421]
24. Bild AH, Yao G, Chang JT, Wang Q, Potti A, Chasse D, et al. Oncogenic pathway signatures in human cancers as a guide to targeted therapies. Nature. 2006; 439(7074):353–7. [PubMed: 16273092]
25. Tibshirani R. The lasso method for variable selection in the Cox model. Stat Med. 1997; 16(4): 385–95. [PubMed: 9044528]
26. Benjamini YHY. Controlling the false discovery rate: a practical and powerful approach to multiple testing. Journal of the Royal Statistical Society, Series B (Statistical Methodology). 1995; 57(1):289–300.
27. Huang da W, Sherman BT, Lempicki RA. Systematic and integrative analysis of large gene lists using DAVID bioinformatics resources. Nat Protoc. 2009; 4(1):44–57. [PubMed: 19131956]
28. Culhane AC, Schwarzl T, Sultana R, Picard KC, Picard SC, Lu TH, et al. GeneSigDB--a curated database of gene expression signatures. Nucleic Acids Res. 2010; 38(Database issue):D716–25. [PubMed: 19934259]
29. Huang da W, Sherman BT, Lempicki RA. Bioinformatics enrichment tools: paths toward the comprehensive functional analysis of large gene lists. Nucleic Acids Res. 2009; 37(1):1–13. [PubMed: 19033363]

30. Croft D, O'Kelly G, Wu G, Haw R, Gillespie M, Matthews L, et al. Reactome: a database of reactions, pathways and biological processes. Nucleic Acids Res. 2011; 39(Database issue):D691–7. [PubMed: 21067998]
31. Hanahan D, Weinberg RA. Hallmarks of cancer: the next generation. Cell. 2011; 144(5):646–74. [PubMed: 21376230]
32. Hirschhaeuser F, Sattler UG, Mueller-Klieser W. Lactate: a metabolic key player in cancer. Cancer Res. 2011; 71(22):6921–5. [PubMed: 22084445]
33. Osborne JR, Port E, Gonen M, Doane A, Yeung H, Gerald W, et al. 18F-FDG PET of locally invasive breast cancer and association of estrogen receptor status with standardized uptake value: microarray and immunohistochemical analysis. J Nucl Med. 2010; 51(4):543–50. [PubMed: 20237034]
34. Palaskas NJ, Larson SM, Schultz N, Komisopoulou E, Wong J, Rohle D, et al. 18F-fluorodeoxy-glucose positron emission tomography (18FDG-PET) marks MYC-overexpressing human basal-like breast cancers. Cancer Res. 2011 Epub 2011/06/08. doi: 10.1158/0008-5472.CAN-10-4633. PubMed PMID: 21646475.
35. Warburg O. On respiratory impairment in cancer cells. Science. 1956; 124(3215):269–70. [PubMed: 13351639]
36. Warburg O. On the origin of cancer cells. Science. 1956; 123(3191):309–14. [PubMed: 13298683]
37. Robey RB, Hay N. Is Akt the “Warburg kinase”?-Akt-energy metabolism interactions and oncogenesis. Semin Cancer Biol. 2009; 19(1):25–31. [PubMed: 19130886]
38. Dang CV. Enigmatic MYC Conducts an Unfolding Systems Biology Symphony. Genes Cancer. 2010; 1(6):526–31. [PubMed: 21218193]
39. Dang CV. Glutaminolysis: supplying carbon or nitrogen or both for cancer cells? Cell Cycle. 2010; 9(19):3884–6. [PubMed: 20948290]
40. Dang CV. Rethinking the Warburg effect with Myc micromanaging glutamine metabolism. Cancer Res. 2010; 70(3):859–62. [PubMed: 20086171]
41. Boellaard R, Krak NC, Hoekstra OS, Lammertsma AA. Effects of noise, image resolution, and ROI definition on the accuracy of standard uptake values: a simulation study. J Nucl Med. 2004; 45(9):1519–27. [PubMed: 15347719]
42. Soret M, Bacharach SL, Buvat I. Partial-volume effect in PET tumor imaging. J Nucl Med. 2007; 48(6):932–45. [PubMed: 17504879]
43. Vesselle H, Freeman JD, Wiens L, Stern J, Nguyen HQ, Hawes SE, et al. Fluorodeoxyglucose uptake of primary non-small cell lung cancer at positron emission tomography: new contrary data on prognostic role. Clin Cancer Res. 2007; 13(11):3255–63. [PubMed: 17545531]
44. Tylski P, Stute S, Grotus N, Doyeux K, Hapdey S, Gardin I, et al. Comparative assessment of methods for estimating tumor volume and standardized uptake value in (18)F-FDG PET. J Nucl Med. 2010; 51(2):268–76. [PubMed: 20080896]
45. Velasquez LM, Boellaard R, Kollia G, Hayes W, Hoekstra OS, Lammertsma AA, et al. Repeatability of 18F-FDG PET in a multicenter phase I study of patients with advanced gastrointestinal malignancies. J Nucl Med. 2009; 50(10):1646–54. [PubMed: 19759105]
46. Bhattacharjee A, Richards WG, Staunton J, Li C, Monti S, Vasa P, et al. Classification of human lung carcinomas by mRNA expression profiling reveals distinct adenocarcinoma subclasses. Proc Natl Acad Sci U S A. 2001; 98(24):13790–5. [PubMed: 11707567]
47. Casali C, Cucca M, Rossi G, Barbieri F, Iacuzio L, Bagni B, et al. The variation of prognostic significance of Maximum Standardized Uptake Value of [18F]-fluoro-2-deoxy-glucose positron emission tomography in different histological subtypes and pathological stages of surgically resected Non-Small Cell Lung Carcinoma. Lung Cancer. 2010; 69(2):187–93. [PubMed: 19942313]

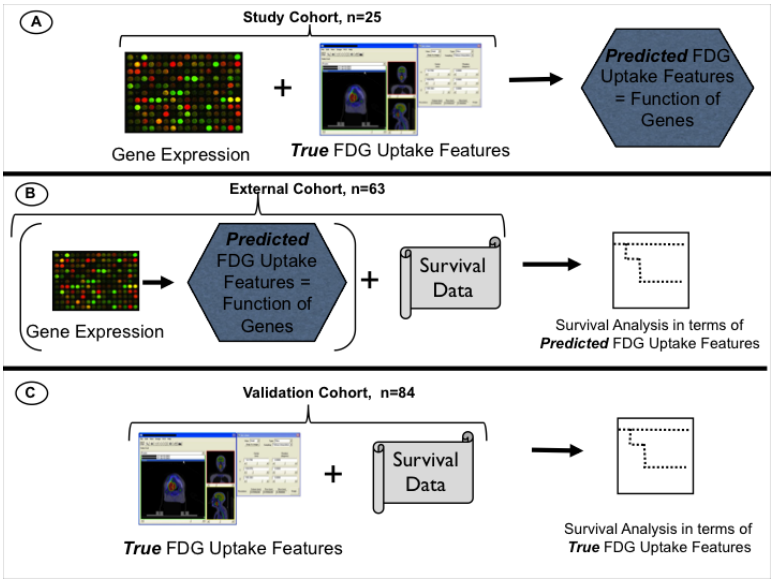

Figure 1. Study design

A) 25 patients with NSCLC and PET imaging prior to resection had genome wide expression performed on cryopreserved tissues (study cohort). FDG uptake features were extracted and predicted in terms of a gene signature. **B)** Predicted FDG uptake features (prefixed by "*p*" in this study) were examined in a second (external) cohort with NSCLC outcome data and gene expression. **C)** Validation of the predicted FDG uptake features that were identified as prognostic in the external cohort was performed in a third (validation) cohort with PET imaging and outcome data to determine if the true FDG uptake features remained significantly associated with overall survival.

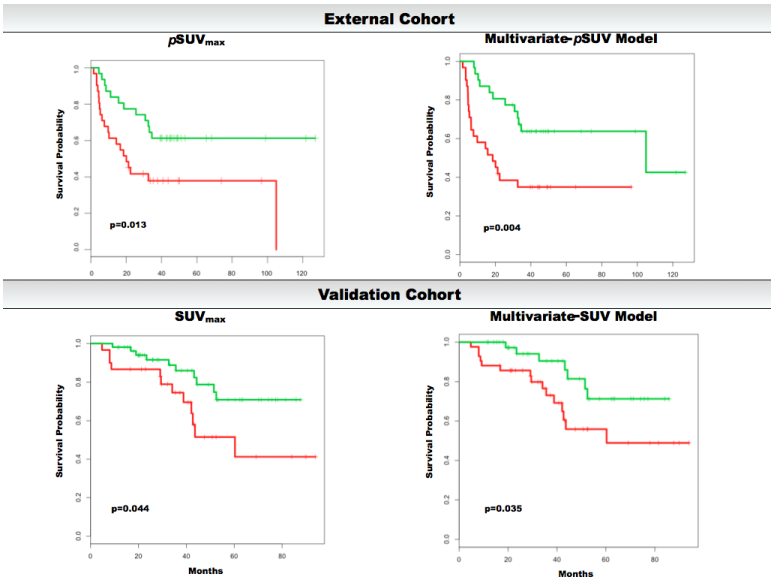

Figure 2. Overall survival for prognostically significant FDG uptake features

Survival analysis demonstrating that SUV_{max} and the multivariate-SUV model were prognostically significant in external and validation cohorts respectively. In the external cohort, the predicted image features (denoted by the prefix "*p*") were assessed. Worse vs. better survival is illustrated by the red vs. green curves. The y-axis represents percent alive and the x-axis is months to event. Note that the x-axis is different for the two cohorts since duration of follow-up time was unique for each cohort. Supplement 5 provides additional plots for prognostic single genes associated with FDG uptake.

Table 1

Characteristics of study and validation cohorts[a]

	Study (n=25)	Validation (n=84)
Age (years)	68 (63–72)	71 (64–77)
Male gender	18 (72)	38 (45)[e]
Ethnicity[b]		
Caucasian	17 (60)	50 (60)
Asian	3 (12)	19 (22)
Other	5 (20)	15 (18)
Tumor diameter (cm)[b]	2.3 (1.7–2.9)	2.5 (1.9–3.8)
Procedure		
Wedge Resection	1 (4)	12 (14)
Lobectomy	24 (96)	61 (72)
Other	0 (0)	11 (13)
Stage		
I-II	24 (96)	84 (100)
III-IV	1 (4)	0 (0)
Histology		
Adenocarcinoma	20 (80)	60 (71)
Squamous	4 (16)	20 (24)
Other	1 (4)	4 (5)
PET to resection time (days)	27 (9–45)	28 (13–47)
Glucose level prior to PET (mg/dL)	106 (100–108)[f]	100 (95–108)
Time to scan (minutes)	60 (60–71)	60 (60–60) [e]
Injected dose (millicuries)	14.5 (12.9–15.8)	14.8 (13.5–16.4)
FDG uptake imaging feature[s]		
Intensity metrics		
SUV_{max}	3.2 (2.6–7.4)	5.9 (3.3–12.1)
SUV_{median}	1.8 (1.5–2.3)	2.6 (1.8–4.2)[e]
SUV_{mean}	1.9 (1.7–2.8)	2.9 (1.9–4.8)
$SUV_{75\%}$	3.4 (1.9–3.4)	3.2 (1.6–5.2)
$SUV_{90\%}$	2.5 (2.2–4.7)	4.3 (2.5–8.1)
SUV_{min}	1.4 (1.2–1.6)	1.8 (1.4–2.4)[e]
Distribution metrics		
$SUV_{kurtosis}$	-0.06 (-0.53–0.61)	-0.14 (-0.60–0.51)
SUV_{skew}	0.87 (0.66–1.2)	0.83 (0.61–1.1)
SUV_{sigma}	0.48 (0.27–1.3)	0.96 (0.47–2.2)
$SUV_{variance}$	0.23 (0.07–1.7)	0.92 (0.22–4.6)
Spatial metrics		

	Study (n=25)	Validation (n=84)
SUV_{MTV} (cm^3)	3.8 (2.0–13)	6.7 (3.5–25)
SUV_{area} (cm^2)	11.6 (4.8–41)	16.6 (8.1–59)
SUV_{points} *c*	67 (26–249)	97 (46–342)
SUV_{TGV} (cm^3) *d*	13 (4.0–30)	22 (8.0–91)

MTV=metabolic tumor volume; TGV=total glycolytic volume.

a Continuous variables are shown with median and interquartile range and categorical variables with number and percent.

b Kurtosis represents “peakedness” of FDG uptake, skew the deviation from a normal distribution, and sigma and variance the breadth of uptake distribution

c Number of voxels used to generate MTV

d Equivalent to the product of SUV_{mean} and SUV_{MTV}

e $p<0.05$ between study and validationcohorts for these variables

f for 10 of 25 patients where data was available.

Table 2

Genes and metagenes associated with FDG uptake features in study cohort[a]

Gene	Functional Annotation	SUV-associated FDG Uptake Feature
BIRC2	Baculoviral IAP repeat containing 2	SUV_{mean}
FAP	Fibroblast activation protein, alpha	SUV_{mean}, SUV_{median}, SUV_{TGV}
FURIN	Paired basic amino acid cleaving enzyme	SUV_{mean}, $SUV_{75th\ percentile}$
LOC648470	Caspase 4, apoptosis-related cysteine peptidase	SUV_{mean}, SUV_{median}
LY6E	Lymphocyte antigen 6 complex, locus E	SUV_{skew}
MCM6	Minichromosome maintenance complex component 6	SUV_{skew}
RNF149	Ring finger protein 149	SUV_{mean}
OBFC1	Oligonucleotide-binding fold containing 1	SUV_{area}, SUV_{MTV}

Metagene[b]	Genes (n)	Functional Annotation[c]	SUV-associated FDG Uptake Feature
Metagene 10	52	Focal and cell adhesion	SUV_{mean}, SUV_{median}, SUV_{TGV}
Metagene 18	36	Protein catabolism	SUV_{max}, $SUV_{variance}$
Metagene 26	18	Nucleic acid processing	SUV_{skew}
Metagene 30	19	Metalloproteinase genes, collagen	SUV_{mean}, SUV_{median}, SUV_{max}
Metagene 70	34	Targets of TP53, RB1	$SUV_{minimum}$
Metagene 78	19	Protein processing	SUV_{TGV}
Metagene 86	34	Embryogenesis, apoptosis	SUV_{max}, SUV_{TGV}
Metagene 100	25	Extracellular matrix, hypoxia and apoptosis	SUV_{max}, SUV_{TGV}

TGV=Total Glycolytic Volume; MTV=Metabolic Tumor Volume.

[a] False discovery rate=0 by SAM, per methods

[b] See Supplement 2 for a full list of genes comprising each metagene

[c] See Supplements 3 and 4 for a full list of enrichment features associated with metagenes.

Table 3

Accuracy of gene signatures that predict FDG uptake features in study cohort[a]

Predicted FDG uptake feature	Accuracy[b]	Meta-genes (n)	Genes (n)
***p*SUV$_{max}$**	0.774	15	508
***p*SUV$_{mean}$**	0.765	13	428
***p*SUV$_{median}$**	0.748	13	428
***p*SUV$_{min}$**	0.762	18	612
***p*SUV$_{90\%}$**	0.765	16	552
***P*SUV$_{75\%}$**	0.777	14	458
***p*SUV$_{sigma}$**	0.765	16	555
***p*SUV$_{variance}$**	0.804	12	387
***p*SUV$_{skew}$**	0.784	14	516
***p*SUV$_{kurtosis}$**	0.725	18	589
***p*SUV$_{area}$**	0.866	11	300
***p*SUV$_{points}$**	0.875	10	270
***p*SUV$_{MTV}$**	0.871	10	270
***p*SUV$_{TGV}$**	0.854	11	315
***p*SUV$_{PCA1}$**	0.793	13	458
***p*SUV$_{PCA2}$**	0.765	16	473

[a] Predicted features are denoted with a prefix "*p*" and are based on a linear combination of genes from the study cohort (see Methods)

[b] Accuracy defined as $1- \Sigma^{25} |pFDGfeature_X\text{-}FDGfeature_X|/\Delta range$.[12]

Table 4

Prognostic significance of genes, metagenes and associated FDG uptake features in external and validation cohorts[a]

Univariate Survival Analysis				
Gene	**Function of Gene**	**HR (95% CI) External Cohort**	**SUV-associated FDG Uptake Feature**	**HR (95% CI) Validation Cohort**
FAP	Fibroblast proliferation and activation	1.45 (1.00-2.09)	SUV_{mean}	1.13 (0.99–1.30)
			SUV_{median}	1.15 (0.98–1.34)
			SUV_{TGV}	1.00 (1.00–1.00)[f]
RNF149	Unknown	2.20 (1.42-3.39)	SUV_{mean}	1.13 (0.99–1.30)
LY6E	Immune recognition and cell trafficking	1.46 (1.04-2.05)	SUV_{skew}	1.69 (0.69–4.11)
MCM6	Genome replication/cell proliferation	1.49 (1.06-2.11)	SUV_{skew}	1.69 (0.69–4.11)

Predicted FDG Uptake Feature	**Functional Enrichment[b,c]**	**HR (95% CI) External Cohort**	**SUV-associated FDG Uptake Feature**	**HR (95% CI) Validation Cohort**
***p*SUV$_{max}$[d]**	Cell cycle and extracellular matrix (ECM)	1.56 (1.07–2.28)	SUV_{max}	1.05 (1.00–1.10)
***p*SUV$_{mean}$[d]**	Cell cycle and immune response	1.55 (1.03–2.33)	SUV_{mean}	1.13 (0.99–1.30)
***p*SUV$_{variance}$[d]**	Cell cycle and ECM	0.69 (0.49–0.97)	$SUV_{variance}$	1.06 (0.99–1.41)
***p*SUV$_{min}$[d]**	Cell signaling and ECM	1.60 (1.03–2.46)	SUV_{min}	1.12 (0.73–1.78)
***p*SUV$_{PCA2}$[d]**	Antigen presentation and processing	1.49 (1.02–2.19)	SUV_{PCA2}	1.24 (0.97–1.59)
Multivariate-*p*SUV[d,e]	Cell/antigen processing, immune response, ECM	5.87 (2.59–13.8)	Multivariate-SUV[e]	6.12 (1.08–34.8)

HR=Hazard Ratio; CI=Confidence Interval

[a] For overall survival, external cohort n=63 and validation cohort n=84. See Supplement 6 for analyses with clinical variables and imaging features

[b] See Supplement 2 for a full list of genes associated with metagenes

[c] See Supplements 3 and 4 for enrichment analysis of gene lists using DAVID and GSEA bioinformatics tools

[d] "*p*" denotes predicted features defined by gene expression and examined in the external cohort

[e] Multivariate expression coefficients for SUV_{max}, $SUV_{variance}$ and SUV_{PCA2} were 0.260, -0.281 and 0.148 respectively

[f] p=0.001